Journal of the European Ceramic Society **18** (1998) 209–219

PII: S0955-2219(97)00116-7
0955-2219/98/$19.00 + 0.00

The Effect of TiO_2 Addition on Strengthening and Toughening in Intragranular Type of 12Ce–TZP/Al_2O_3 Nanocomposites

Masahiro Nawa,[a]* Noriko Bamba,[b] Tohru Sekino[b] and Koichi Niihara[b]

[a]Central Research Laboratory, Matsushita Electric Works, Ltd., 1048, Kadoma, Osaka 571, Japan
[b]The Institute of Scientific and Industrial Research, Osaka University, 8-1, Mihogaoka, Ibaraki, Osaka 567, Japan

(Received 18 March 1997; accepted 30 May 1997)

Abstract

To compensate the definite disadvantages of lower strength and lower hardness in Ce–TZP, an intragranular type of 12Ce–TZP/0–30 vol% Al_2O_3 nanocomposite was investigated. Furthermore, the effect of TiO_2 addition on strengthening and toughening was also examined for the optimum component of 30 vol% Al_2O_3, which showed a maximum strength of 866 MPa. For these composites, a novel interpenetrated intragranular microstructure was presented, in which either 200-nm-sized Al_2O_3 particles or 30–50-nm-sized ZrO_2 particles were trapped within the ZrO_2 grains or Al_2O_3 grains, respectively. The TiO_2 was confirmed to dissolve into the tetragonal ZrO_2 lattice, and contributed to the phase stability of the tetragonal phase and the promotion of intragranular nano-dispersion. For the small amount (0·2 mol%) of TiO_2 doped 12Ce–TZP/30 vol% Al_2O_3 composite, simultaneous improvements in strength (1012 MPa) and toughness (10·2 MPa·$m^{1/2}$ for the IF method, 5·7 MPa·$m^{1/2}$ for the SEVNB method) were achieved through tailoring the sintering condition. © *1997 Elsevier Science Limited.*

1 Introduction

In various ceramics, tetragonal zirconia polycrystals (TZP), stabilized with Y_2O_3 (Y–TZP) or CeO_2 (Ce–TZP), has been tailored to achieve either a high strength or a high toughness.[1–3] However, the attractive property of the TZP and/or TZP based composite is apparently accompanied by either a modest toughness for Y–TZP or a modest strength for Ce–TZP. For instance, Ce–TZP containing 8–12 mol% CeO_2[3] have exhibited fairly high toughness values of 10–20 MPa.$m^{1/2}$, but show hardness value of 8 GPa and strength values of only 600–800 MPa even for an optimum CeO_2 content of 12 mol%. On the other side, Y–TZP are currently applying for a wide industry use due to their well-balanced high tolerance for catastrophic fracture. However, they have an essential fault suffering from low-temperature aging degradation in strength at around 200°C.[4] Conversely, Ce–TZP have a complete resistance to low-temperature aging degradation[5] although they have definite disadvantages of both lower strength and lower hardness in comparison to those of Y–TZP. Consequently, if Ce–TZP successfully achieved both high strength and high hardness, they would be expected as the candidate for a new attractive TZP ceramic, which overcomes low-temperature aging degradation of Y–TZP.

To compensate the disadvantages of lower strength and lower hardness in Ce–TZP, recent investigations have been focused on Ce–TZP/Al_2O_3 composite system. In the 12 mol% Ce–TZP (12Ce–TZP) based composites containing 30–50 vol% Al_2O_3, strength has improved up to 900 MPa. However, toughness decreased remarkably from 20 to 5·5 MPa·$m^{1/2}$ with increasing Al_2O_3 content.[6] Thus, it was proved that further addition of the second phase resulted in the inevitable decrease of the toughness due mainly to the restraint of the tetragonal-to-monoclinic transformation. To restrain the toughness degradation of the composite caused by the addition of the second phase, the form controls of Al_2O_3 particles have been investigated. It was shown that the toughness can be improved by incorporation of the elongated and/or plate-like Al_2O_3 phases which were produced in

*To whom correspondence should be addressed.

situ sintering by the addition of small amount of metal oxides[7,8] or dispersing lanthanim–aluminate crystals.[9] However, the formations of micrometer sized elongated and/or plate-like second phases were not always effective to improve the strength due to the enlargement of a flaw size in the composites. Therefore, it is a serious point of contention whether or not the flaw size can be restrained successfully in order to improve strength in the Ce–TZP/Al_2O_3 composite system.

In recent years, nanocomposites, in which nanometer sized second phase particles are dispersed within the ceramic matrix grains and/or at the grain boundaries, have been investigated in an attempt to eliminate the strength-degrading flaws.[10,11] They have shown significant improvements in strength and creep resistance even at high temperatures. However, regarding the toughness, the nanocomposites showed a modest improvement in comparison with that of other conventional ceramic composites.

The purpose of this investigation is to apply a general idea of the nanocomposite to Ce–TZP/Al_2O_3 composite system, and to confirm the possibility for further strengthening while still preserving high toughness. In this study, we tried to fabricate an intragranular type of Ce–TZP/Al_2O_3 nanocomposite, in which fine Al_2O_3 particles are dispersed within the zirconia grains. Furthermore, the effect of TiO_2 addition on strengthening and toughening was investigated. In the zirconia-rich end of the titania phase equilibrium diagram,[12] TiO_2 is known to dissolve into tetragonal ZrO_2 up to 18 mol% at high temperatures and act as a stabilizing agent in the similar manner to Y_2O_3 and CeO_2. Furthermore, TiO_2 is well known to promote a grain growth of ceramic. For example, 10 mol% TiO_2 doped 8Y–TZP ceramic showed the transparent property due to a homogeneous and large grain growth by the addition of TiO_2.[13] Therefore, it is expected that TiO_2 additions to the Ce–TZP/Al_2O_3 composite system would be effective for strengthening from the point of the phase stability of the tetragonal phase and the promotion of intragranular nano-dispersion due to its ability to promote grain growth.

First, we have tried to fabricate an intragranular type of nanocomposites and to confirm the possibility for strengthening of the 12Ce–TZP/Al_2O_3 composites containing 0–30 vol% Al_2O_3. The effect of TiO_2 content on further strengthening has been examined for the optimum component of the 12Ce–TZP/30 vol% Al_2O_3 composites, which showed a maximum strength. The relationship between microstructure and mechanical properties will be discussed.

2 Experimental procedure

2.1 Fabrication

Ce–TZP powder containing 12 mol% CeO_2 (grade TZ-12CE, Tosoh Co., Japan) with a specific surface area of 10 $m^2 g^{-1}$ and TiO_2 powder (grade SP-01, Osaka Titanium Co., Japan) with a specific surface area of 25 $m^2 g^{-1}$ were used as a starting material for the matrix. γ–Al_2O_3 powder (grade TM-300, Taimei Chemical Co., Japan) with a specific surface area of 270 $m^2 g^{-1}$ was used as the secondary dispersions. For all three powders, the base 12Ce–TZP powder with addition of either 0, 0·2, 0·5, 1 or 3 mol% TiO_2 and appropriate amounts of Al_2O_3 dispersions were ball milled using zirconia milling media in ethanol for 24 h. Then the mixtures were dried in air and calcined at 1000°C for 1 h to dissolve TiO_2 into ZrO_2 and coalesce γ–Al_2O_3 powder. Calcined powders were further milled in ethanol for 24 h and dried and passed through a 250-μm screen. For all powder mixtures, green compacts were prepared by first uniaxial die pressing at 10 MPa and isostatic pressing at 150 MPa. The common sintering conditions were 1500–1650°C for 2 h.

2.2 Characterizations

The densities of the specimens were obtained by the Archimedes method using a toluene medium. Crystalline phases of the composites on the polished surfaces of the specimens were determined by X-ray diffraction analysis (XRD) with CuKα radiation. The tetragonal, monoclinic and cubic phases were evaluated using the analysis of Garvie and Nicholson[14] and the volume fraction of the monoclinic phase was determined using the equation of Toraya *et al.*[15] Lattice constants of the tetragonal ZrO_2 for the 0–3 mol% TiO_2 doped 12Ce–TZP/30 vol% Al_2O_3 composites were determined by XRD with CrKα radiation based on the outer standard method using Si powder. The grain size of the composite was estimated by the line intercept method on the thermally etched surfaces. The microstructure of the composites was observed by scanning electron microscopy (SEM) and transmission electron microscopy (TEM).

2.3 Mechanical properties

The sintered specimens were cut by a diamond blade saw, and ground with a 600-grit diamond wheel. The specimens, having dimensions of 3×4×40 mm, were subjected to the elastic modulus measurement and mechanical property tests. The elastic modulus was determined by the resonance vibration method. The fracture strength was measured by a 3-point bending test at room temperature. The span length and cross-head speed were

30 mm and 0·5 mm min^{-1}, respectively. The tensile surfaces of the specimens were polished with a diamond liquid suspension. The fracture toughness was estimated by the indentation-fracture (IF) method using the following equation of Niihara *et al.*[16]

$$K_{IC} = 0{\cdot}018 Hv\, a^{1/2}\, (l/a)^{-1/2}\, (H_v/E)^{-2/5}$$

where H_v is the Vickers hardness and E is the elastic modulus. Here, $l = c - a$, wherein a and c are the half length of the Vickers impression and the palmquist crack, respectively. The polished surfaces were used for the Vickers indentation with a load of 490 N and a loading duration of 15 s. Separately, the toughness was also estimated by the single edge V notched beam (SEVNB) method. The V notch was machined using a special diamond slicing wheel, which was developed by Awaji *et al.*[17] The required toughness can be accurately obtained by forming a sharper V-shaped notch with very small root curvature. In this study, the specimens, having a V notch root radius around 10 to 15 μm, were used. The V notched specimens, having dimensions of 3×4×20 mm, were subjected to a 3-point bending test with a span length of 16 mm and a cross-head speed of 0·5 mm min^{-1}. The value of toughness was calculated by using Srawley's shape coefficient.[18]

3 Results and Discussion

3.1 Microstructure

12Ce–TZP/0–30 vol% Al_2O_3 composites sintered at various temperatures were composed of only ZrO_2 and Al_2O_3. No crystalline reaction phases were detected. The ZrO_2 matrix in these composites consisted primarily of the tetragonal phase and a small amount (less than 1 vol%) of the monoclinic phase. There were no traces of the cubic phase. In the system of 0–3 mol% TiO_2 doping 12Ce–TZP/30 vol% Al_2O_3 composites, the identical crystalline phases were detected.

The variations of average grain size of ZrO_2 matrix with Al_2O_3 content are shown in Fig. 1. Here, the 12Ce–TZP/Al_2O_3 composites, containing 0, 5, 20 and 30 vol% Al_2O_3, were sintered at 1500, 1550, 1600 and 1650°C for 2 h. It was confirmed that the addition of Al_2O_3 particles remarkably inhibited grain growth of ZrO_2 matrix even in a small addition. Next, the representative microstructures of the 12Ce–TZP/0–30 vol% Al_2O_3 composites, sintered at 1600°C, are shown in Fig. 2. They were characterized by SEM using polished surfaces that were thermally etched in air for 30 min at the temperature below 50°C for each sintering conditions. In the small range (less than 5 vol%) of Al_2O_3 content, the intragranular microstructure was observed, in which the submicron sized Al_2O_3 particles of about 0·3 μm were dispersed within the 3–4-μm-sized ZrO_2 grains. With increasing Al_2O_3 content up to 30 vol%, the slight grain growth of Al_2O_3 particles was observed, whereas the remarkable inhibition of ZrO_2 grain growth was occurred. As a result, it is predicted that the trapping ratio of Al_2O_3 particles to the ZrO_2 grains has been decreased. However, it was recognized that the intragranular nano-dispersion was still presented in the composites.

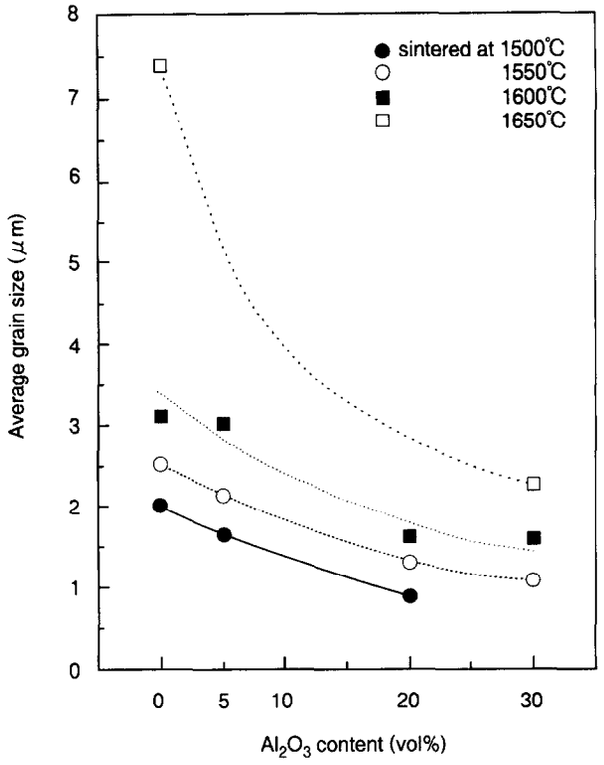

Fig. 1. The variations of average grain size of ZrO_2 matrix with Al_2O_3 content for the 12Ce–TZP/0–30 vol% Al_2O_3 composites.

A characteristic TEM image of the 0·2 mol% TiO_2 doped 12Ce–TZP/30 vol% Al_2O_3 composite, sintered at 1600°C, is shown in Fig. 3. It was recognized that a novel interpenetrated intragranular type of nano-dispersion[19] was presented in the 12Ce–TZP/Al_2O_3 composite system. That is, either 200-nm-sized Al_2O_3 particles or 30–50-nm-sized ZrO_2 particles were trapped within the ZrO_2 grains or Al_2O_3 grains, respectively. On the other hand, the identical microstructure was also observed in the without TiO_2 doping 12Ce–TZP/Al_2O_3 composite system.

3.2 Mechanical properties

3.2.1 The effect of Al_2O_3 dispersion

The variation of the fracture strength with the Al_2O_3 content for the 12Ce–TZP/0–30 vol% Al_2O_3

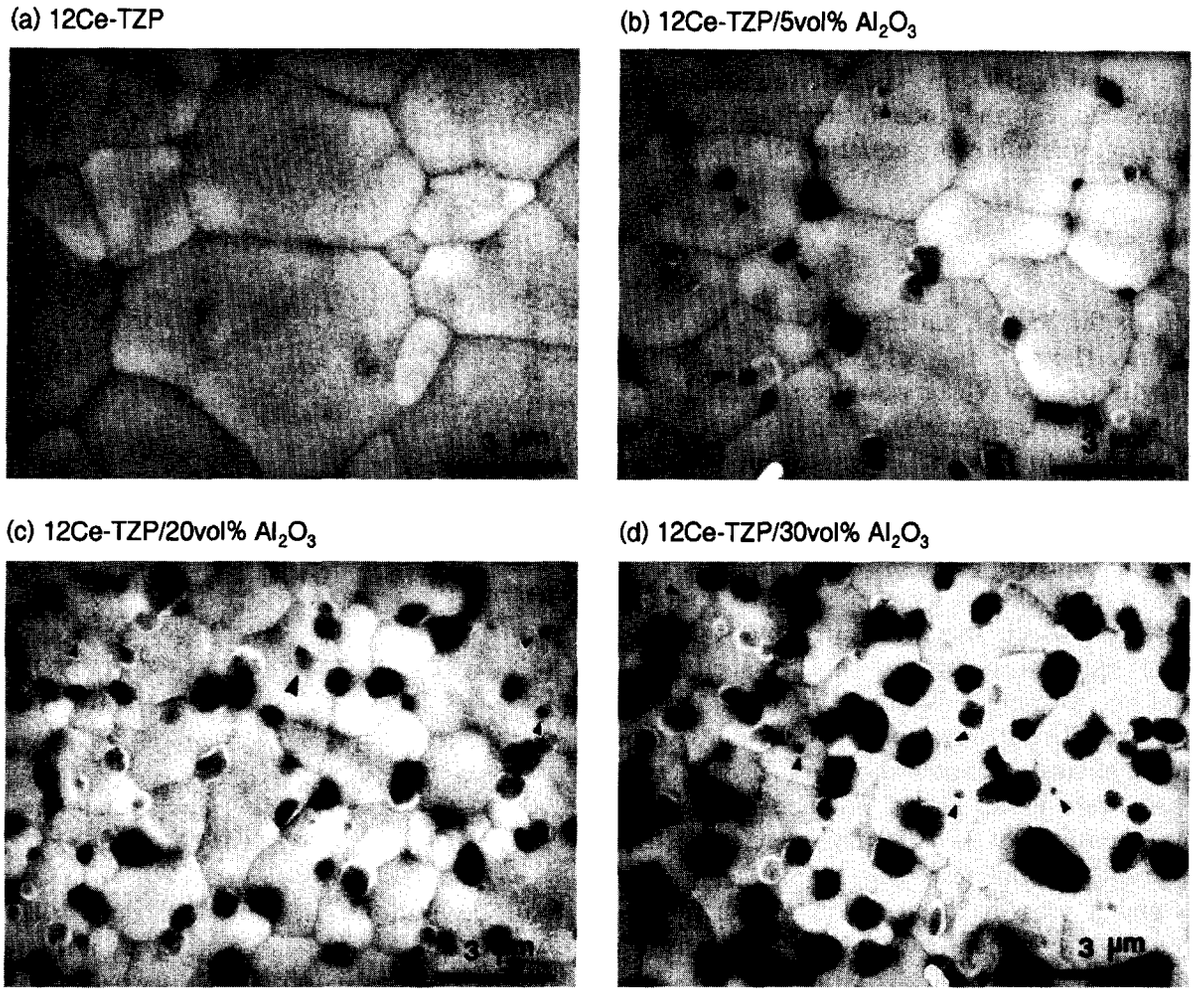

Fig. 2. SEM photographs of representative microstructures for the 12Ce–TZP/(a) 0, (b) 5, (c) 20, (d) 30 vol% Al_2O_3 composites sintered at 1600°C.

composites is shown in Fig. 4. The strength increased with increasing Al_2O_3 content up to 30 vol%, and a maximum value of 866 MPa was obtained for the 12Ce–TZP/30 vol% Al_2O_3 composite sintered at 1600°C. This strengthening was determined to be the result of two separate constituents. The first concems a decrease in flaw size relating a reduction of the grain size for both the ZrO_2 and the Al_2O_3 grains. In fact, the grain size of the ZrO_2 matrix (approximately 7·5 μm for the monolithic ZrO_2 sintered at 1650°C) was reduced to 2.5 μm by the addition of 30 vol% of Al_2O_3 particles (see Fig. 1). Furthermore, associated with the interpenetrated intragranular nano-dispersion, several 10–100-nm-sized inclusions, which are trapped inside the ZrO_2 and/or Al_2O_3 grains, are believed to have a role in dividing a grain size into more finer sized particles by forming sub-grain boundaries.[11] The second constituent concerns the stress induced phase transformation on strengthening for TZP ceramics. It has been determined that the retention of the tetragonal phase is critically governed by the grain size.[1] That is, reduction of the grain size is predicted to increase the critical stress that induces the tetragonal-to-monoclinic transformation. It has become apparent that the increase of the critical stress leads to augmentation of the strength of TZP ceramics.[20] As describe above, these interactive contributions are considered to result in the improvement of the strength.

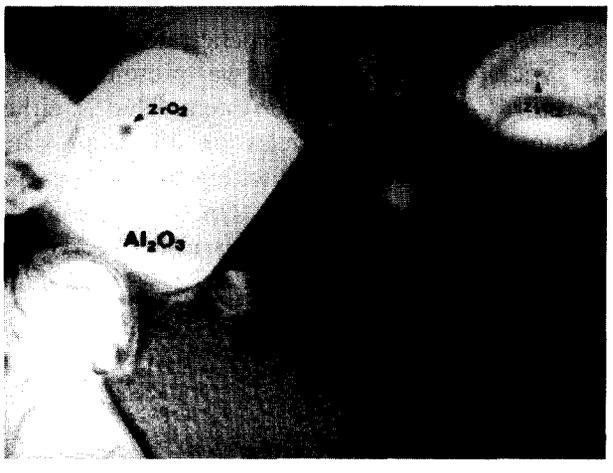

Fig. 3. TEM image of the 0·2 mol% TiO_2 doped 12Ce–TZP/30 vol% Al_2O_3 composite sintered at 1600°C.

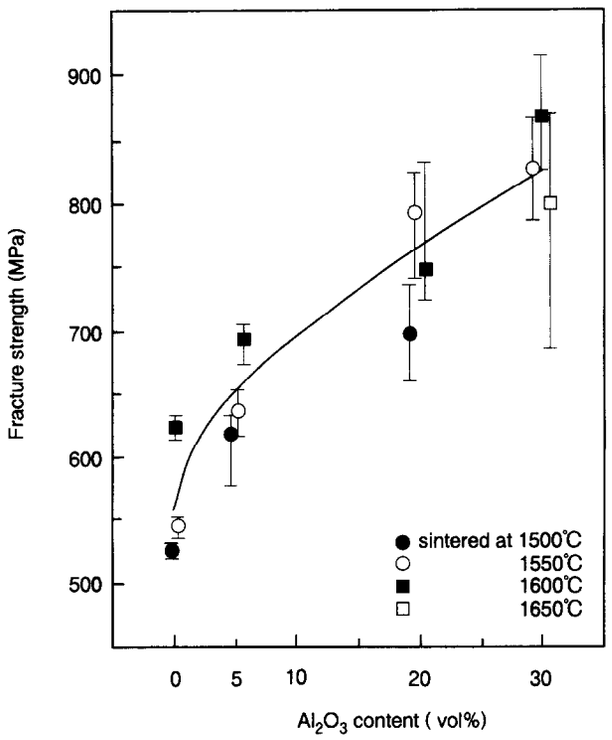

Fig. 4. The variation of the fracture strength with the Al_2O_3 content for the 12Ce–TZP/0–30 vol% Al_2O_3 composites.

The variation of the fracture toughness with the Al_2O_3 content, which was both evaluated by the IF method and the SEVNB method, is shown in Fig. 5. For the Ce–TZP ceramics, the values of the toughness estimated by the IF method may be disposed to overestimate due to the large transformed zone about the Vickers impression[21] and the elongated transformed zone forming ahead of the crack tip.[22,23] To confirm above notion, the transformation zone developed about a 490 N Vickers indent was examined by using the optical polarized microscope. The Nomarski interference images of the indent for the 12Ce–TZP/0, 20 and 30 vol% Al_2O_3 composites are shown in Fig. 6. For the monolithic 12Ce–TZP, it was confirmed that the

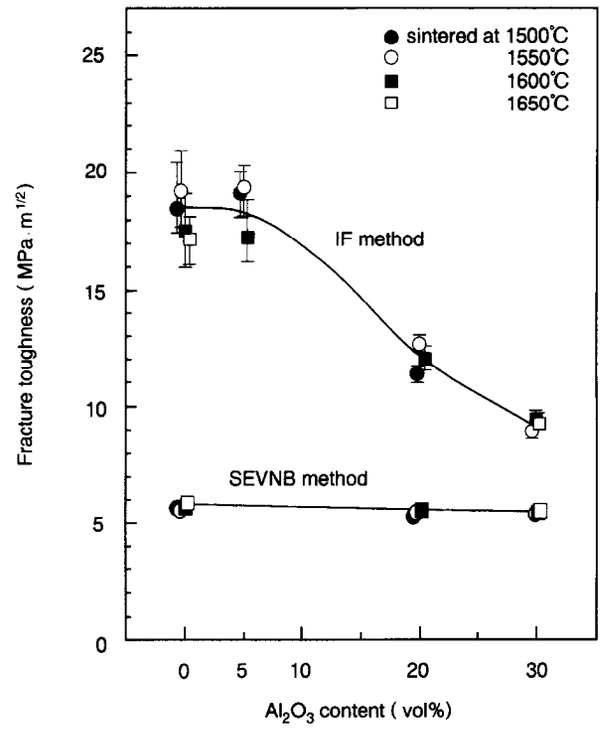

Fig. 5. The variation of the fracture toughness with the Al_2O_3 content, which was evaluated by both the IF method and the SEVNB method, for the 12Ce–TZP/0–30 vol% Al_2O_3 composites.

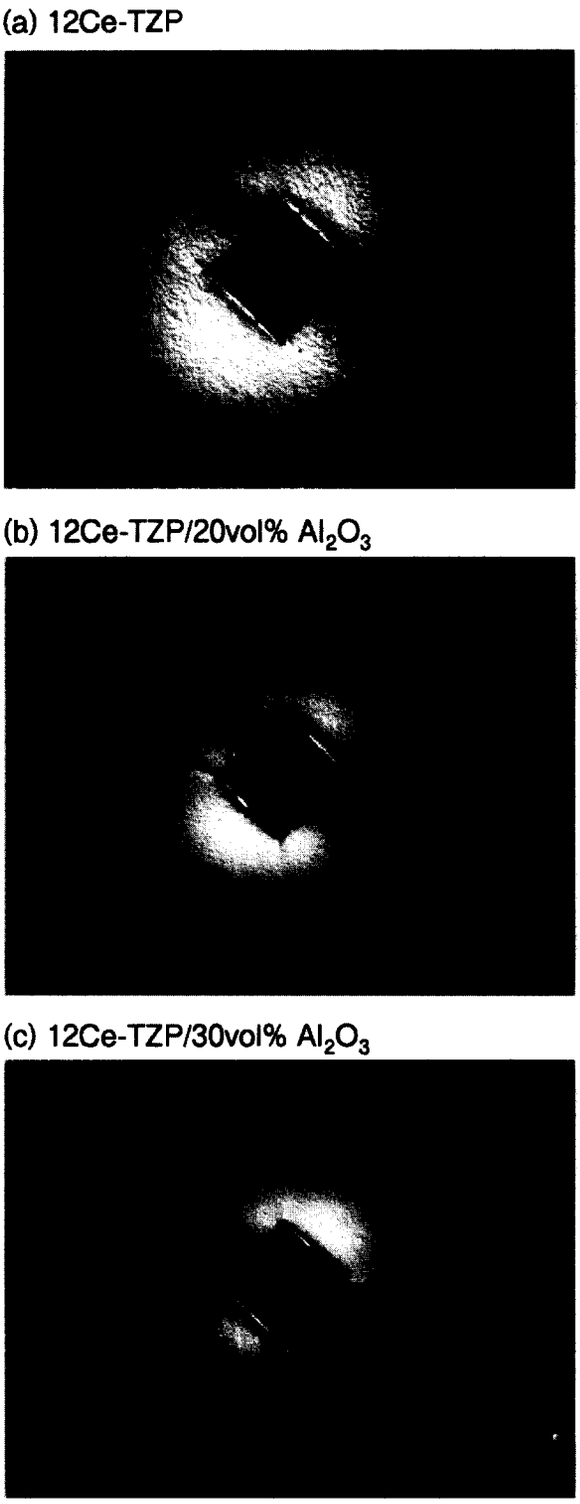

Fig. 6. Optical micrographs of the transformation zone (Nomarski interference image) developed about a 490 N Vickers indent for the 12Ce–TZP/Al_2O_3 composites containing (a) 0, (b) 20, (c) 30 vol% Al_2O_3, respectively.

large developed transformation zone was recognized. On the contrary, with increasing Al_2O_3 content up to 30 vol%, the transformed zone size was apparently decreased. Next, the influence of the toughness value on the applied load is shown in Fig. 7 for the monolithic 12Ce–TZP and the composite containing 30 vol% Al_2O_3. The increase of the toughness was observed with increasing applied load for the monolithic 12Ce–TZP, which might be due to the rising R-curve behavior.[24] On the other hand, the dependence of the toughness on the applied load was not identified for the 12Ce–TZP/30 vol% Al_2O_3 composite. Consequently, it was concluded that the toughness estimated by the IF method, especially for the monolithic 12Ce–TZP, might correspond to the increased stage of toughness in its strong rising R-curve, which was governed by the well developed process zone. The volume fraction of the monoclinic phase in both polished and fractured surfaces, as a function of Al_2O_3 content for the 12Ce–TZP/0–30 vol% Al_2O_3 composites, is shown in Fig. 8. The monoclinic phase in the fractured surface showed a remarkable decrease from 60 to 7 vol% with the addition of Al_2O_3 up to 30 vol%. Judging from above results, it is predicted that the toughness will extremely decrease with increasing Al_2O_3 content. In the IF method, a serious decrease from 18·1 to 9·0 MPa·$m^{1/2}$ was recognized with increasing Al_2O_3 content. On the other hand, the toughness measured by the SEVNB method exhibited almost the same value about 5 MPa·$m^{1/2}$ independently of the Al_2O_3 content. This behavior revealed no exact correspondence to a remarkable decrease of the transformed monoclinic phase. The toughness estimated by the SEVNB method has been verified to evaluate a crack initiation behavior by eliminating rising R-curve behavior.[17] By comparing the toughness obtained by the IF method, it is reasonable to conclude that the reduction of tetragonal-to-monoclinic transformation might be corresponded to the disappearance of rising R-curve behavior by the addition of Al_2O_3 particles.

The variations of Vickers hardness and elastic modulus with Al_2O_3 content for the 12Ce–TZP/0–30 vol% Al_2O_3 composites are shown in Fig. 9. In the Vickers hardness, the calculated value by the linear rule of mixtures was shown as the dotted line using the experimental data of the monolithic 12Ce–TZP (8 GPa) and Al_2O_3 polycrystal (18·5 GPa). For the elastic modulus, a solid line linking both ends corresponded to the relation of the linear rule of mixtures, in which the elastic modulus of Al_2O_3 polycrystal suppose to be 350 GPa. As shown in Fig. 9, the variation of each coefficient with Al_2O_3 content was demonstrated to be in good agreement with the predicted changes by the linear rule of mixtures. In the case of the Vickers hardness, however, a slight hardening was recognized in the 5 vol% Al_2O_3 content.

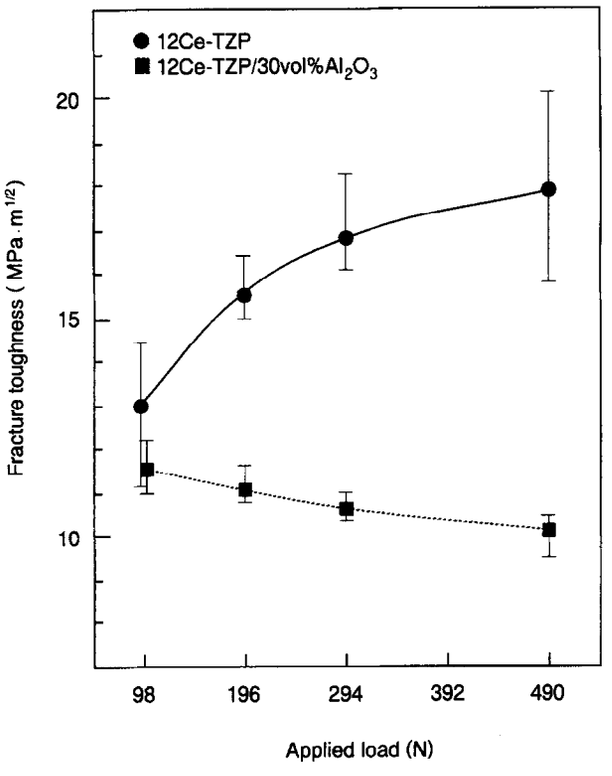

Fig. 7. The variation of the fracture toughness with applied load, which evaluated by the IF method, for both the monolithic 12Ce–TZP and the composite containing 30 vol% Al_2O_3 sintered at 1600°C for 2 h.

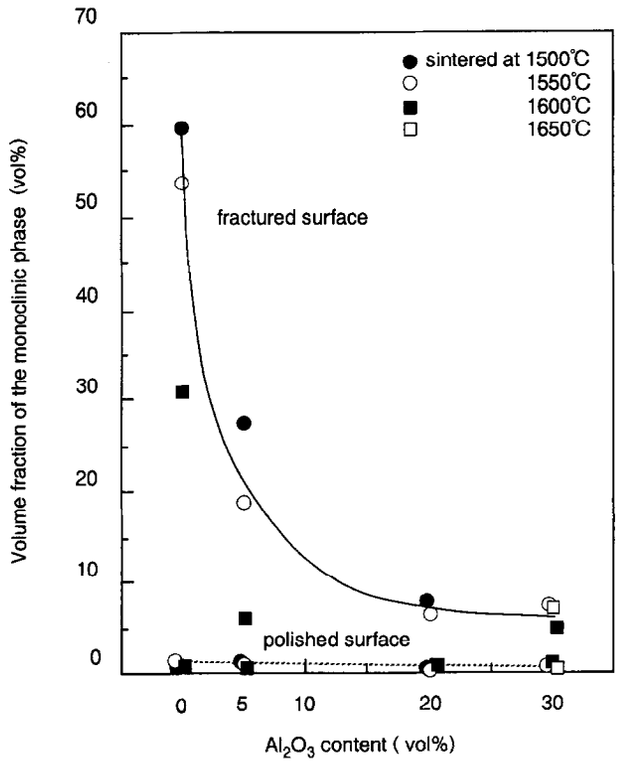

Fig. 8. The volume fraction of the monoclinic phase in both polished and fractured surfaces as a function of Al_2O_3 content for the 12Ce–TZP/0–30 vol% Al_2O_3 composites.

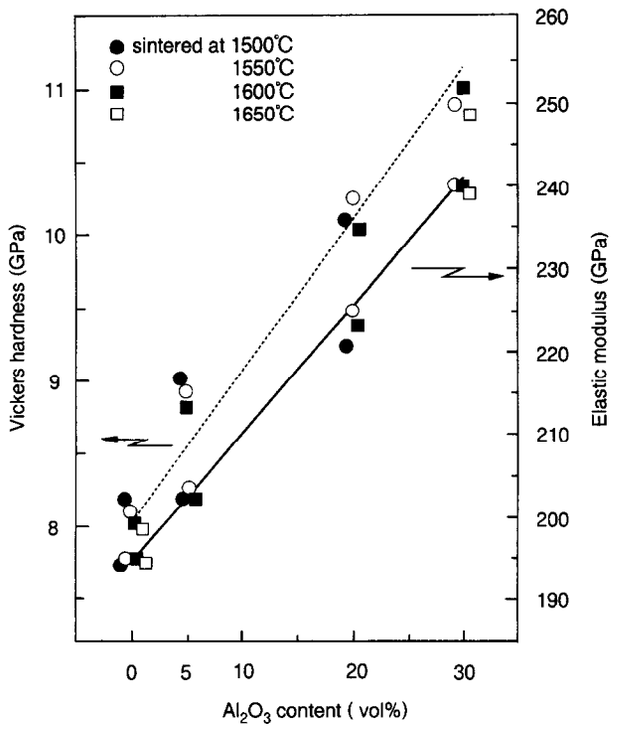

Fig. 9. The variation of the Vickers hardness and the elastic modulus with Al_2O_3 content for the 12Ce–TZP/0–30 vol% Al_2O_3 composites.

3.2.2 The effect of TiO_2 doping

The effect of TiO_2 addition (0, 0·2, 0·5, 1 and 3 mol%) on further strengthening was examined for the optimum component of the 12Ce–TZP/30 vol% Al_2O_3 composites, which showed a maximum strength of 866 MPa. Furthermore, additional sintering condition of 1650°C for 10 h was also examined to investigate the effect of holding time at sintering temperature on strengthening and toughening for both systems of 12Ce–TZP/30 vol% Al_2O_3 with (0.2 mol%) and without TiO_2 doping.

The lattice constant, the axial ratio and the lattice volume of the tetragonal ZrO_2, for the 0–3 mol% TiO_2 doped 12Ce–TZP/30 vol% Al_2O_3 composites sintered at 1650°C for 2 h and 10 h, are presented in Table 1. It was shown that both lattice constants and lattice volumes of the tetragonal ZrOz decreased with increasing TiO_2 content. These results reveal that a titania ion, having a smaller ionic radius than those of Zr^{4+} and/or Ce^{4+}, dissolved into the tetragonal ZrO_2 lattice, although the exact configuration of this solid solution is not clear. According to above analysis, it seemed reasonable to presume that TiO_2 addition to the Ce–TZP/Al_2O_3 composite would be effective for strengthening from the phase stability of the tetragonal phase due to its ability to act as a stabilizing agent.

The density as a function of TiO_2 content for the 12Ce–TZP/30 vol% Al_2O_3 composites is shown in Fig. 10. The density decreased with increasing TiO_2 content and with rising sintering temperature, especially above 1 mol% TiO_2 content. This degradation was believed to be responsible for the solid solution of TiO_2 ion into the tetragonal ZrO_2 lattice.

The fracture strength as a function of TiO_2 content for the 12Ce–TZP/30 vol% Al_2O_3 composites is shown in Fig. 11. The strength slightly increased with increasing small amount of TiO_2 doping. Especially, the strength showed a characteristic increase with a small amount (0·2 mol%) of TiO_2 content, and a maximum value of 949 MPa was obtained for the sintering condition of 1650°C for 2 h. In addition, further improvement of the strength up to 1012 MPa was achieved by only extending the holding time from 2 to 10 h. Above-mentioned strengthening was also found for the without TiO_2 doping of identical composite. The variation of the average grain size of the ZrO_2 matrix with various sintering conditions was summarized in Table 2 for the 12Ce–TZP/30 vol% Al_2O_3 composites with (0·2 mol%) and without TiO_2 doping. The average grain size were gradually increased with rising sintering temperature and with extending holding time for both systems. Hence, it was ascertained that TiO_2 had an ability to enhance a grain growth on ZrO_2 matrix. Therefore, TiO_2 was supposed to act as a sintering aid and to contribute to a promotion of the

Table 1. The lattice constant and axial ratio of tetragonal ZrO_2 for the 0–3 mol% TiO_2 doped 12Ce–TZP/30 vol% Al_2O_3 composites sintered at 1650°C for 2 h and 10 h

	a, b (Å)	c *(Å)*	$c/\sqrt{2}a$	*Volume (nm^3)*
Sintering condition of 1650°C for 2 h				
12Ce–TZP/30 vol% Al_2O_3 composite	3·6306 (+0·0002)*	5·2327 (+0.0005)*	1·0191	$68{\cdot}973\times10^{-3}$
0·2 mol% TiO_2 doping of above composite	3·6289 (+0·0007)	5·2335 (+0·0015)	1·0198	$68{\cdot}920\times10^{-3}$
0·5 mol% TiO_2 doped	3·6268 (+0·0003)	5·2296 (+0·0007)	1·0196	$68{\cdot}788\times10^{-3}$
1·0 mol% TiO_2 doped	3·6227 (+0·0004)	5·2254 (+0·0009)	1·0199	$68{\cdot}576\times10^{-3}$
3·0 mol% TiO_2 doped	3·6211 (+0·0008)	5·2203 (+0·0018)	1·0194	$68{\cdot}451\times10^{-3}$
Sintering condition of 1650°C for 10 h				
12Ce–TZP/30 vol% Al_2O_3 composite	3·6303 (+0·0005)	5·2321 (+0·0010)	1·0191	$68{\cdot}954\times10^{-3}$
0·2 mol% TiO_2 doping of above composite	3·6274 (+0·0008)	5·2311 (+0·0017)	1·0197	$68{\cdot}831\times10^{-3}$

*Standard deviation within parentheses.

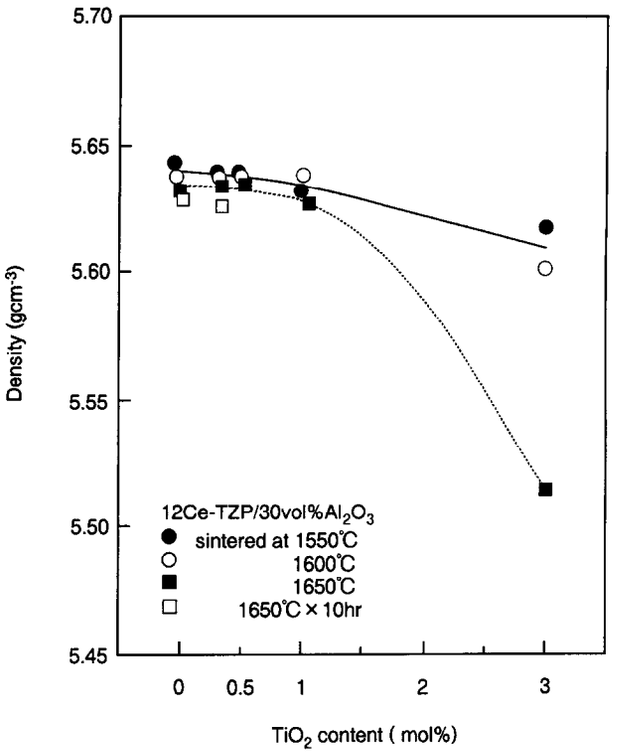

Fig. 10. The density as a function of TiO_2 content for the 12Ce–TZP/30 vol% Al_2O_3 composites sintered at various conditions. The solid line represents the variation of the results taken at all sintering temperatures except for 1650°C, while the dotted line shows the variation of the result of 1650°C.

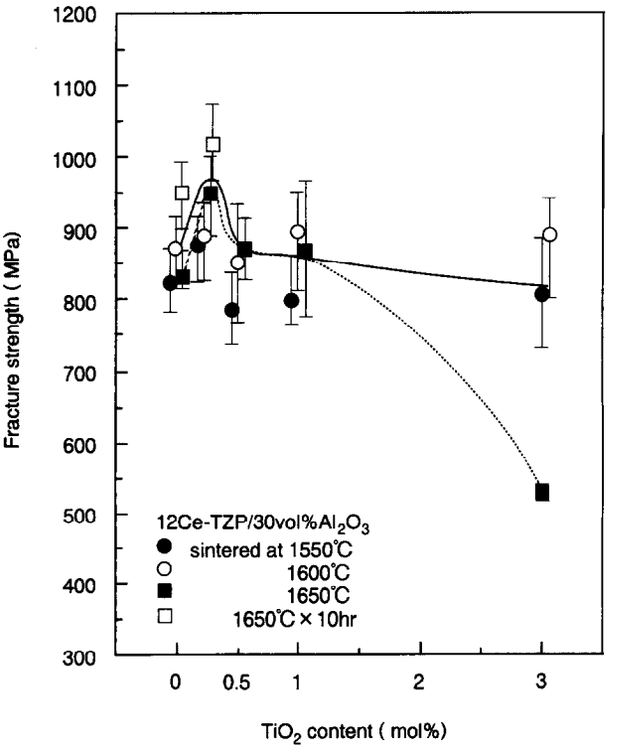

Fig. 11. The fracture strength as a function of TiO_2 content for the 12Ce–TZP/30 vol% Al_2O_3 composites sintered at various conditions. The solid line represents the variation of the results taken at all sintering temperatures except for 1650°C, while the dotted line shows the variation of the result of 1650°C.

intragranular nano-dispersion (Fig. 3). Consequently, the above interactive contributions on TiO_2 addition, concerning the phase stability of the tetragonal phase and the promotion of intragranular nano-dispersion, are considered to result in the improvement of the strength. Meanwhile, in the range above 1 mol% TiO_2 content, the strength had a inclination to decrease with rising sintering temperature and exhibited a remarkable decrease for the 3 mol% TiO_2 doping composite sintered at 1650°C for 2 h. Therefore, it was apparent that an excessive TiO_2 addition above 1 mol% caused a fatal strength degradation due to an extraordinary grain growth of ZrO_2.

The fracture toughness as a function of TiO_2 content, which was both evaluated by the IF method and the SEVNB method, for the 0–3 mol% TiO_2 doped 12Ce–TZP/30 vol% Al_2O_3 composites is shown in Fig. 12. In the IF method, the radical decrease of the toughness was observed in the range from 0·2 to 1 mol% TiO_2 content. After that, the monotonous decrease continued up to 3 mol% TiO_2 content. These results revealed that TiO_2 had a role in restraint of the tetragonal-to-monoclinic transformation, which was based on TiO_2 ion dissolved into the tetragonal ZrO_2 lattice. As the exceptional case, 3 mol% TiO_2 doped composite sintered at 1650°C for 2 h exhibited a high toughness value of 9·2 MPa·$m^{1/2}$. The variation of transformation zone developed about a 490 N Vickers indent with sintering temperature (1550°C, 1600°C, 1650°C) as shown in Fig. 13. The apparent grain growth and enlargement of the transformed zone size was observed with rising sintering temperature. Therefore, this toughening behavior was concluded to be derived from the promotion of the tetragonal-to-monoclinic transformation due to the large grain growth. The toughness measured by the SEVNB method showed a similar result, although the ratio of the variation was small.

On the contrary, a significant increase of the toughness (8·6–10·2 MPa·$m^{1/2}$ for the IF method, and 5·3–5·7 MPa·$m^{1/2}$ for the SEVNB method) was recognized by extending holding time at 1650°C from 2 to 10 h for the 0·2 mol% TiO_2 doped 12Ce–TZP/30 vol% Al_2O_3 composite, and without TiO_2 doping of identical composite. The TEM image of the intragranular microstructure of the ZrO_2 grain, for the 0·2 mol% TiO_2 doped 12Ce–TZP/30 vol% Al_2O_3 composite sintered at 1650°C for 10 h, is shown in Fig. 14. A number of the different nanometer-sized precipitation were observed inside the ZrO_2 grain. The composition of such found in tiny phase could not be identified. The inference here is probably that the solid solution of CeO_2 might be in the stage of its reduction into Ce_2O_3 due to the change of the valence level

Table 2. The variation of the average grain size of the ZrO_2 matrix with various sintering conditions for the 12Ce–TZP/30 vol% Al_2O_3 composites with (0.2 mol%) and without TiO_2 doping

Sintering conditions	*1550°C×2 h*	*1600°C×2 h*	*1650°C×2 h*	*1650°C×10 h*
Average grain size (μm)				
12Ce–TZP/30 vol% Al_2O_3 composite	1·11	1·61	2·26	3·12
0·2 mol% TiO_2 doping of above composite	1·20	1·81	2·49	3·29

from Ce^{4+} to Ce^{3+} influenced by rising sintering temperature.[25] When the above phenomenon occurs one of the Ce^{4+} ion, having a larger ionic radius than that of Zr^{4+}, would be transferred to Ce^{3+}, and precipitated as Ce_2O_3. As a result, CeO_2 content should decrease a little from 12 mol% and will result in the decrease of the lattice constant. As shown in Table 1, a little decrease of the lattice constant was recognized in the case when holding time at 1650°C extended from 2 to 10 h. These results can be interpreted as one of the facts supporting the above assumption. Meanwhile, Tsukuma *et al.*[3] reported that the toughness increased with decreasing CeO_2 content for the system of 8–12 mol% Ce–TZP. Consequently, this toughening is considered to result in the slight decrease of CeO_2 content from 12 mol%. The argument remains, however, that accurate analysis of the variation of CeO_2 content should be examined.

The Elastic modulus and the Vickers hardness, as a function of TiO_2 content for the 12Ce–TZP/30 vol% Al_2O_3 composites, are shown in Figs 15 and 16, respectively. Both coefficients showed a

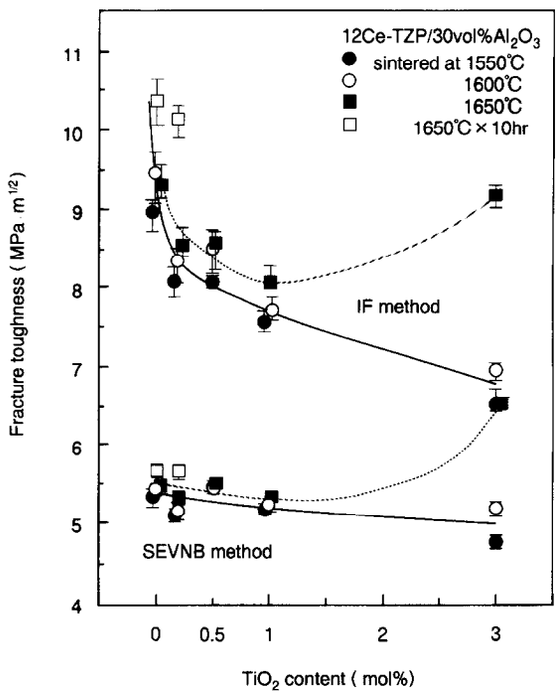

Fig. 12. The fracture toughness as a function of TiO_2 content, which was evaluated by both the IF method and the SEVNB method, for the 12Ce–TZP/30 vol% Al_2O_3 composites. The solid line represents the variation of the results taken at all sintering temperatures except for 1650°C, while the dotted line shows the variation of the result of 1650°C.

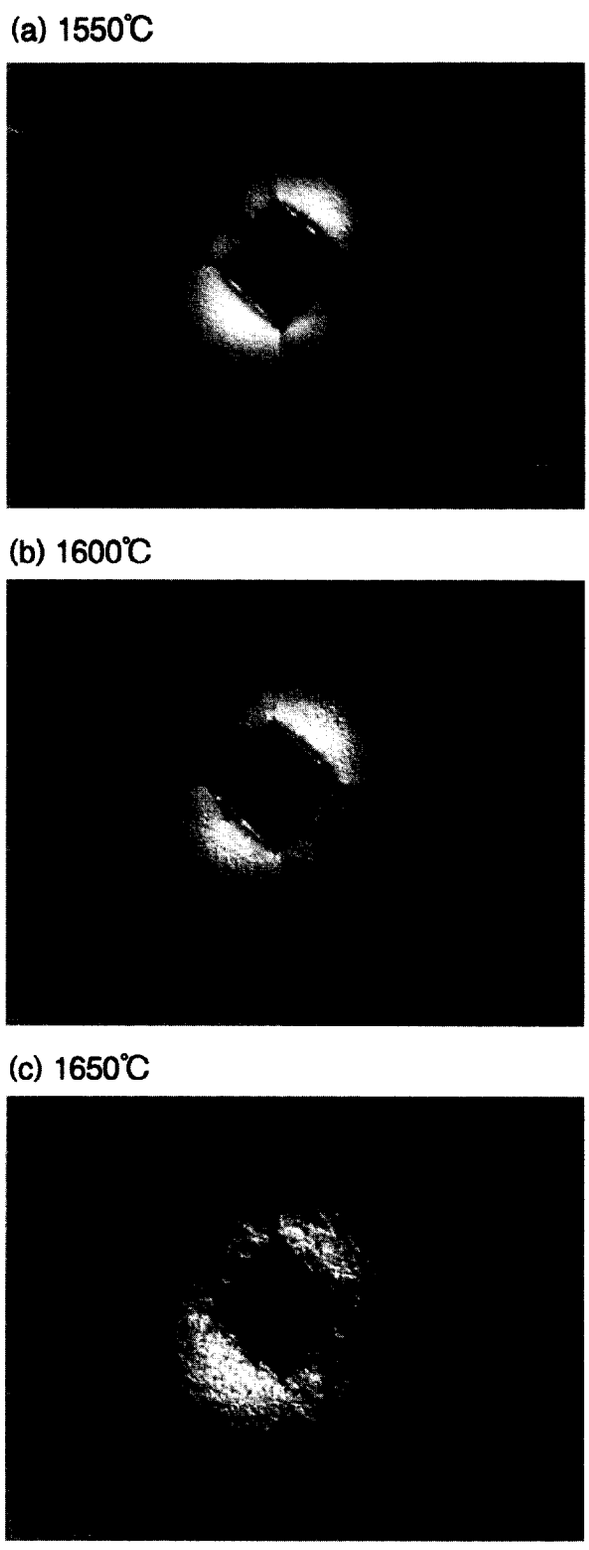

Fig. 13. Optical micrographs of the transformation zone (Nomarski interference image) developed about a 490 N Vickers indent for the 3 mol% TiO_2 doped 12Ce–TZP/Al_2O_3 composites sintered at (a) 1550°C, (b) 1600°C, (c) 1650°C for 2 h.

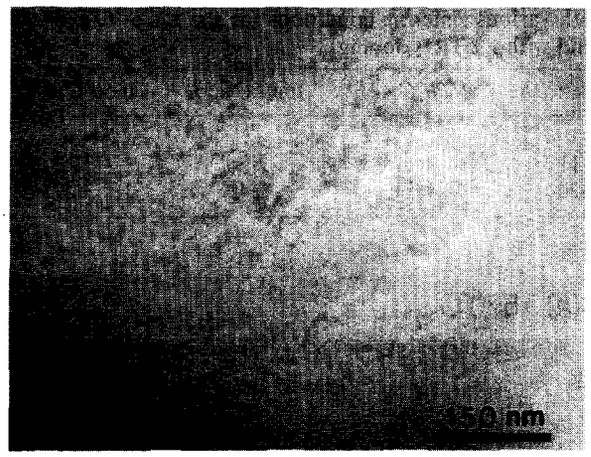

Fig. 14. The TEM image of the intragranular microstructure within the ZrO_2 grain for the 0·2 mol% TiO_2 doped 12Ce–TZP/30 vol% Al_2O_3 composite sintered at 1650°C for 10 h.

decrease inclination with increasing TiO_2 content and with rising sintering temperature. The degradation of the elastic modulus may be attributed to the solid solution of TiO_2 ion into the tetragonal ZrO_2 lattice, which is the equivalent manner recognizing on the deterioration in the density. In the case of the Vickers hardness, however, a slight hardening was observed in the range from 0·2 to 0·5 mol% TiO_2 content, which corresponded to the component exhibiting a maximum strength. This accordance was believed to be associated with a promotion of the intragranular nano-dispersion, which was derived from a small amount of TiO_2 addition.

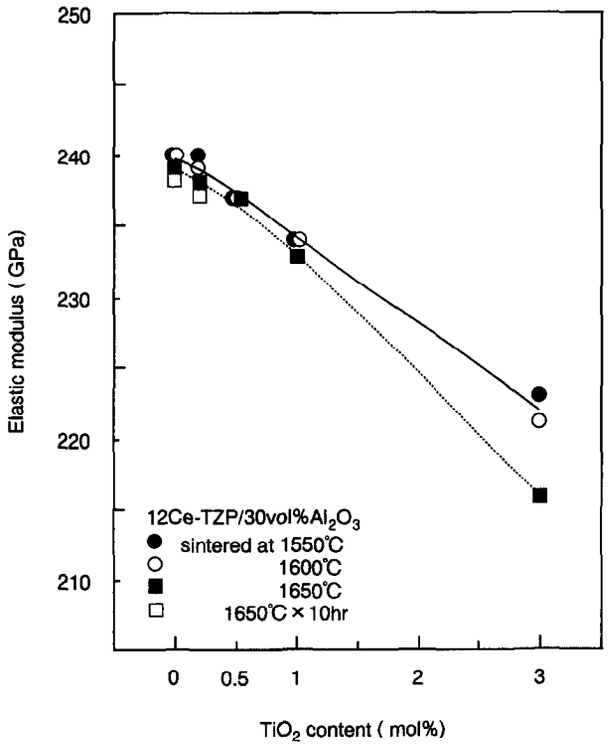

Fig. 15. The elastic modulus as a function of TiO_2 content for the 12Ce–TZP/30 vol% Al_2O_3 composites sintered at various conditions. The solid line represents the variation of the results taken at all sintering temperatures except for 1650°C, while the dotted line shows the variation of the result of 1650°C.

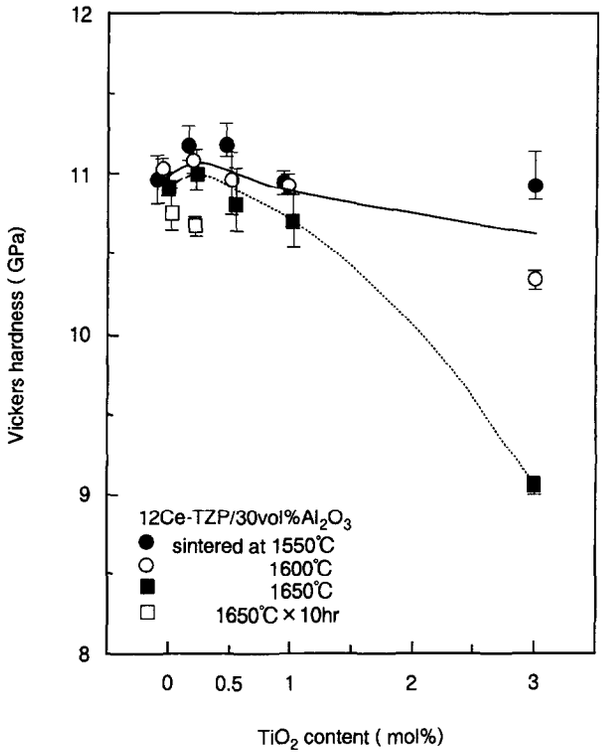

Fig. 16. The Vickers hardness as a function of TiO_2 content for the 12Ce–TZP/30 vol% Al_2O_3 composites sintered at various conditions. The solid line represents the variation of the results taken at all sintering temperatures except for 1650°C, while the dotted line shows the variation of the result of 1650°C.

4 Conclusions

To compensate the definite disadvantages of lower strength and lower hardness in Ce–TZP, we investigated an intragranular type of 12Ce–TZP based nanocomposite containing 0–30 vol% Al_2O_3. In addition, the effect of TiO_2 addition on further strengthening was also examined for the optimum component of 30 vol% Al_2O_3. The microstructures and their mechanical properties were studied. The results are summarized as follows.

1. 12Ce–TZP/0–30 vol% Al_2O_3 composites sintered at various temperatures were composed of only ZrO_2 and Al_2O_3. The ZrO_2 matrix in these composites consisted primarily of the tetragonal phase and a small amount of the monoclinic phase. There were no traces of the cubic phase. In the system of 0–3 mol% TiO_2 doping 12Ce–TZP/30 vol% Al_2O_3 composites, the identical crystalline phases were detected. The TiO_2 was confirmed to dissolve into the tetragonal ZrO_2 lattice, and contributed to the

phase stability of the tetragonal phase and the promotion of intragranular nano-dispersion due to its grain growth enhancing ability on ZrO_2.

2. For the 12Ce–TZP/Al_2O_3 composites with and without TiO_2 doping, the intragranular nanostructure was presented, in which the submicron szed Al_2O_3 particles of about 0·3 μm were dispersed within the 3–4-μm-sized ZrO_2 grains. Furthermore, they partly possessed a novel interpenetrated intragranular microstructure, in which either 200-nm-sized Al_2O_3 particles or 30–50-nm-sized ZrO_2 particles were trapped within the ZrO_2 grains or Al_2O_3 grains, respectively.
3. A small amount (0·2 mol%) of TiO_2 added to the optimum component of 12Ce–TZP/30 vol% Al_2O_3 composite, that exhibited a maximum strength of 866 MPa, resulted in further strengthening up to 949 MPa. In addition, through tailoring the sintering condition by extending a holding time at higher sintering temperature, a significant improvement on the strength of 1012 MPa was achieved. Moreover, simultaneous improvement of the toughness (10·2 MPa·$m^{1/2}$ for the IF method, and 5·7 MPa·$m^{1/2}$ for the SEVNB method) was presented due to the acceleration of the tetragonal-to-monoclinic transformation, although an excessive TiO_2 addition above 1 mol% caused a fatal strength and toughness degradation.

References

1. Gupta, T. K., Lange, F. F. and Bechtold, J. H., Effect of stress-induced phase transformation on the properties of polycrystalline zirconia containing metastable tetragonal phase. *J. Mater. Sci.*, 1978, **13**, 1464–1470.
2. Masaki, T., Mechanical properties of toughened ZrO_2–$Y2O_3$ ceramics. *J. Am. Ceram. Soc.*, 1986, **69**, 638–640.
3. Tsukuma, K. and Shimada, M., Strength, fracture toughness and Vickers hardness of CeO_2-stabilized tetragonal ZrO_2 polycrystals (Ce–TZP). *J. Mater. Sci.*, 1985, **20**, 1178–1184.
4. Masaki, T., Mechanical properties of Y-PSZ after aging at low temperature. *Int. J. High Technol. Ceram.*, 1986, **2**, 85–98.
5. Tsukuma, K., Mechanical properties and thermal stability of CeO_2 containing tetragonal zirconia polycrystals. *Am. Ceram. Soc. Bull.*, 1986, **65**, 1386–1389.
6. Tsukuma, K., Takahata, T. and Shiomi, M., In *Advances in Ceramics, 24, Science and Technology of Zirconia III.* The American Ceramic Society, Westerville, OH, 1988, pp. 721–728.
7. Tsai, J. F., Chon, U., Ramachandran, N. and Shetty, D. K., Transformation plasticity and toughening in CeO_2-partially-stabilized zirconia–alumina (Ce–TZP/Al_2O_3) composites doped with MnO. *J. Am. Ceram. Soc.*, 1992, **75**, 1229–1238.
8. Culter, R. A., Mayhew, R. J., Prettyman, K. M. and Virkar, A. V., High-toughness Ce–TZP/Al_2O_3 ceramics with improved hardness and strength. *J. Am. Ceram. Soc.*, 1991, **74**, 179–186.
9. Miura, M., Hongoh, H., Yogo, T., Hirano, S. and Fujii, T., Formation of plate-like lanthanum–aluminate crystal in Ce–TZP matrix. *J. Mater. Sci.*, 1994, **29**, 262–268.
10. Niihara, K., Nakahira, A. and Hirai, T., High temperature properties of Al_2O_3–SiC composites. In *Fracture Mechanics of Ceramics* 7, ed. R. C. Bradt, A. G. Evans, D. P. H. Hasselman and F. F. Lange. Plenum Press, New York, 1985, pp. 103–116.
11. Niihara, K., New design concept of structural ceramics—ceramic nanocomposites. *J. Ceram. Soc. Jpn.*, 1991, **99**, 974–982.
12. Brown, F. H. and Duwez, P., The zirconia–titania system. *J. Am. Ceram. Soc.*, 1954, **37**, 129–132.
13. Tsukuma, K., In *Zirconia Ceramics* 8, ed. S. Somia and M. Yoshimura. Uchida Rokakuho, Japan, 1986, pp. 11–20.
14. Garvie, R. C. and Nicholson, P. S., Phase analysis in zirconia systems. *J. Am. Ceram. Soc.*, 1972, **55**, 303–305.
15. Toraya, H., Yoshimura, M. and Somiya, S., Calibration curve for quantitative analysis of the monoclinic-tetragonal ZrO_2 system by X-ray diffraction. *J. Am. Ceram. Soc.*, 1984, **67**, C119–C121.
16. Niihara, K., Morena, R. and Hasselman, D. P. H., Further reply to 'Comment on elastic/plastic indentation damage in ceramics: the median/radial crack system'. *J. Am. Ceram. Soc.*, 1982, **65**, C116.
17. Awaji, H., Watanabe, T. and Sakaida, Y., Fracture toughness measurement of ceramics by V notch technique. *Ceram. Int.*, 1992, **18**, 11–17.
18. Srawley, J. E., Wide range stress intensity factor expressions for ASTM E 399 standard fracture toughness specimens. *Int. J. Fract.*, 1976, **12**, 475–476.
19. Nawa, M., Yamazaki, K., Sekino, T. and Niihara, K., Microstructure and mechanical behaviour of 3Y–TZP/Mo nanocomposites possessing a novel interpenetrated intragranular microstructure. *J. Mater. Sci.*, 1996, **31**, 2849–2858.
20. Swain, M. V. and Rose, L. R. F., Strength limitations of transformation-toughened zirconia alloys. *J. Am. Ceram. Soc.*, 1986, **69**, 511–518.
21. Hannink, R. H. J., Muddle, B. C. and Swain, M. V., Transformation induced plasticity in tetragonal zirconia polycrystals. *Proc. Austceram 86, Australian Ceram. Soc.*, Melbourne, 1986, p. 145.
22. Rose, L. R. F. and Swain, M. V., Transformation zone shape in ceria-partially-stabilized zirconia. *Acta Metall.*, 1988, **36**, 955–962.
23. Yu, C. S., Shetty, D. K., Shaw, M. C. and Marshall, D. B., Transformation zone shape effects on crack shielding in ceria-partially-stabilized zirconia (Ce–TZP)–alumina composites. *J. Am. Ceram. Soc.*, 1992, **75**, 2991–2994.
24. Minato, I., Pezzotti, G. and Niihara, K., Microstructure and fracture behavior of Si_3N_4 based ceramic composites. *J. Jpn. Soc. Powder and Powder Metall.*, 1992, **39**, 1076–1079.
25. Roth, R. S, Negas, T. and Cook, L. P., *Phase Diagram for Ceramists*, Volume IV. The American Ceramic Society, 1981, Fig. 5001.